

Electron subband degeneracy heat pump for cryogenic cooling

Chulin Wang,^{1, a)} Thomas Douglas,^{1, a)} and Matthew A Grayson¹

Department of Electrical and Computer Engineering, Northwestern University, Evanston, IL 60208

(*Electronic mail: m-grayson@northwestern.edu.)

(Dated: 7 February 2023)

An unconventional method of continuous solid-state cryogenic cooling utilizing the electron subband degeneracy of semiconductor heterostructures is proposed in this Letter. An electrostatic heat pump is modeled, which employs subband “expansion” and “compression” to reach sub-dilution refrigeration temperatures with the fundamental limit set by electron-phonon interaction. Using an ultra-wide GaAs quantum well as an example, the cooling power per unit volume is estimated to reach 4.5 mW/cm^3 with a hot-side temperature of 300 mK, suitable for applications such as quantum computers or infrared detectors.

I. INTRODUCTION

Sustainable and efficient millikelvin cryogenic cooling is essential for supporting cutting-edge applications such as solid-state quantum computation as well as other low-temperature experiments that require low temperatures such as infrared detectors^{1,2} or quantum states with long coherence times such as the quantum Hall effect³. To achieve millikelvin temperatures, one of the most common technologies is the $^3\text{He}/^4\text{He}$ dilution refrigerator⁴. However, since ^3He is a scarce and non-renewable resource, alternative approaches for achieving millikelvin temperatures are greatly desired. Demagnetization refrigeration using polarizable salts only partly solves the problem, since it requires an ancillary multi-Tesla superconducting electromagnet with accompanying power-supply, cryogenic system, and troublesome stray fields^{5,6}. Furthermore, the indirect nature of electron cooling via these phononic refrigeration mechanisms suffers from the notoriously weak coupling of electrons to cooled phonons. A large Kapitza-like thermal resistance⁷ develops between electron and phonon baths due to the vanishing electron-phonon coupling at lower temperatures, meaning that the base temperature of the electron system is frequently much higher than that of the nominal dilution refrigerator base temperature.

In this Letter, a novel approach for sustained cooling is proposed that utilizes electrons, themselves, directly as the refrigeration medium⁸. Just as a dilution refrigerator expands the phase-space of ^3He in the $^3\text{He}/^4\text{He}$ mixture from a low entropy-per-particle state (the concentrated phase) to a high-entropy-per-particle state (the dilute phase) to achieve cooling, this work proposes a novel solid state heat pump that will expand the phase space of a two-dimensional electron system (2DES) from one to multiple subbands to generate cooling power. As a direct means of cooling electrons, this compact mechanism could realize low electron temperatures competitive with standard but cumbersome cryogenic methods. Under this proposal, the weak coupling of phonons and electrons at extreme low temperature becomes an *advantage*, as it eliminates one possible source of heat leak to the cold electrons from hot phonons. Realizing a solid-state active cooling

mechanism at the coldest end of the temperature spectrum will reduce the volume of solid-state cryocoolers by orders of magnitude, increase hold times and improve thermal stability allowing active compensation of heat leaks. The parasitic heat losses for the proposed solid-state refrigerator decrease rapidly at lower temperatures, so this refrigeration method has no fundamental low-temperature limit. Since coherence times typically increase with decreasing temperature⁹, this may help to extend quantum coherence for solid-state quantum information storage.

II. DEVICE DESIGN

The solid state heat pump is based on a semiconductor heterostructure with tunable quantum well subband occupancy. This is achieved via metal gates on both front and back surfaces. Rego and Kirczenow¹⁰ first theoretically proposed that under single-shot operation of front and back gate biasing, the electron subband degeneracy g of the 2DES can be increased without changing the electron density, and as such, the temperature is adiabatically decreased by the same degeneracy factor ratio. However, in their proposed single-shot operation no heat is removed from the 2DES and the drop in temperature is rapidly recovered through contact with the phonon heat bath. The present work extends beyond this proposal, where here a *cyclic heat pump* operating according to the thermodynamic Otto cycle of a heat engine, achieves sustained cryogenic cooling power. Whereas a standard heat pump uses a working medium of molecular gas or liquid manipulated by mechanical pistons and thermal switches, in this Letter, a working medium of electrons in a quantum well is manipulated by electrostatic gates and electron heat-switch gates. The cyclic disconnecting of electrical conduction via capacitive heat-switches allows the Wiedemann-Franz law to be side-stepped, since there never exists a continuous path of electrical conduction from the cold load across the central 2DES to the heat bath.

Figure 1a shows a schematic of the proposed device. The electrons that function as the working medium for refrigeration are in the central region (purple) of the quantum well at variable temperature T_M . The front and back gates are biased to voltages V_F and V_B , which are referred to as the piston gates for compression and expansion analogous to the mechanical

^{a)}These two authors contributed equally

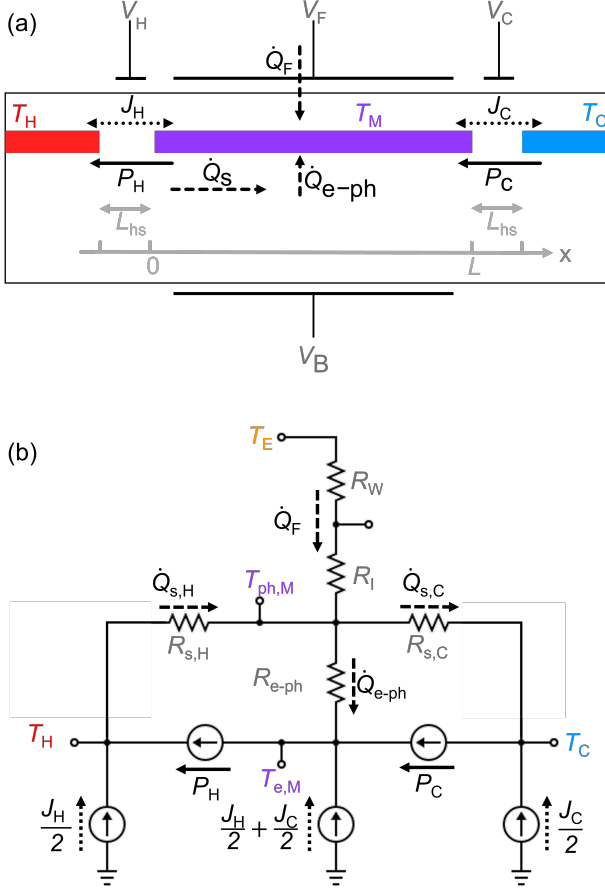


FIG. 1. Subband degeneracy heat pump schematic and equivalent thermal circuit. (a) The electron gas in the central quantum well region of length L (purple) functions as the working medium at variable temperature T_M . This working medium is expanded/compressed into high/low subband degeneracy with the front and back piston gates V_F and V_B , respectively. Cooling power (solid arrows) is pumped from the cold load to the working medium, P_C and ejected from the working medium into the heat sink, P_H . Fourier heat (dashed arrows) flows to the electrons of the working medium from the front and back gates, together labelled as \dot{Q}_F , and from electron-phonon coupling \dot{Q}_{e-ph} within the QW. Additional Fourier heat reaches the cold-side via back-flow of heat through substrate phonons \dot{Q}_S . Temperatures of electrons (e) and phonons (ph) are designated with subscripts, with an additional subscript H, C, and M indicating hot side, cold side, and middle (working medium region) respectively. Joule heating (dotted arrows) at the cold side J_C and hot side J_H occurs in the 2DES when the heat switch gate capacitors are charged and discharged throughout the cooling cycle with V_H and V_C , respectively. (b) Thermal “circuit” equivalent of proposed subband degeneracy refrigerator used for device simulations. Here “currents” represent heat flow following the same notation as panel (a). The environment at T_E connects through the thermal resistance of the electrical wires R_W in series with the insulating layers R_I surrounding the QW, into the phonons in the middle region, $T_{ph,M}$. The phonon reservoirs are connected via back-flow of heat through the thermal resistance of the substrate, R_S . Electron-phonon coupling is modeled with the thermal resistance R_{e-ph} in each region.

heat pump. As such, the piston gates serve to cyclically compress the electrons to low subband degeneracy g_1 or to expand the electrons to high subband degeneracy g_2 . The heat switch gates biased with voltages V_H and V_C can electrostatically deplete the electrons that connect the working medium to the hot and cold sides, respectively, so that direct electronic conduction of heat across the entire device is inhibited throughout the refrigeration cycle. The various heat flows in Fig. 1a are indicated with arrows, indicating the predominant direction of heat flow under proper operation, where the solid black arrows indicate cooling power, dashed arrows represent Fourier heat flow from high to low temperature, and dotted arrows represent Joule heating from the depletion and repopulation of the 2DEG under the heat-switch gates. The thermal equivalent “circuit” is drawn in Fig. 1b to aid in analysis, where temperatures are represented as “voltages”, heat flow as “current”, and thermal resistance as electrical “resistors”. Wires that connect to the gate terminals as well as the gate metals themselves will be made of superconductor, such as aluminum, whose electronic thermal conductivity is negligible, eliminating the heat leak through those electrical contacts^{11,12}. Normal metal wires, such as gold, will connect the hot side of the device to the external heat sink and the cold side to the load to-be-cooled to achieve good thermal contact to those respective electron baths..

III. WORKING PRINCIPLE

The cooling power is generated by operating the working medium of electrons in an Otto cycle¹³. Figure 2 shows this T - S diagram, which is comprised of adiabatic expansion, isochoric heating, adiabatic compression, and isochoric cooling. Here the isochoric legs represent constant subband degeneracy g . The two $T(S)$ curves for degenerate electron systems with different subband degeneracy, g , can be obtained via Sommerfeld expansion¹⁴ and are plotted in blue solid lines in Fig. 2,

$$S = \frac{\pi m^* k_B^2 A_{QW}}{3\hbar^2} g T_e = K g T_e, \quad (1)$$

where g , m^* , k_B , A_{QW} , and T_e represent the electron subband degeneracy factor, effective mass, Boltzmann constant, quantum well area, and electron working medium temperature, respectively. The parameter K in the right-hand equation is defined, $K \equiv \pi m^* k_B^2 A_{QW} / (3\hbar^2)$, which is material-dependent only through the electron effective mass m^* and geometry dependent only through the device area A_{QW} .

The four legs of the Otto cycle can be described as follows, with the inset reproductions of Fig. 1 in miniature illustrating the heat switch positions for each case. (A) Both heat switches are disconnected. The temperature of the working medium drops from T_H to $(g_1/g_2)T_H$ via an adiabatic expansion by biasing the front and back piston gates. (B) The V_C heat switch shown on the right is connected, coupling the working medium to the cold load at T_C , and heat is drawn away from the cold load to the working medium as the working medium undergoes isochoric heating. (C) Adiabatic compression is achieved by biasing the piston gates appropriately with both heat switches

disconnected, and the temperature of the working medium is increased from T_C to $(g_2/g_1)T_C$. (D) Finally, the working medium undergoes isochoric cooling from $(g_2/g_1)T_C$ to T_H , ejecting heat to the heat sink through the V_H heat switch on the left.

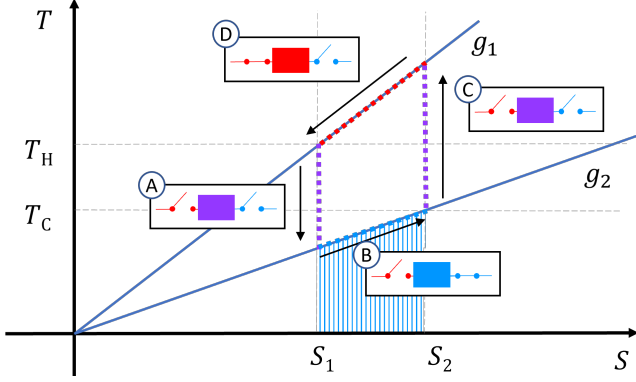


FIG. 2. T - S diagram of the Otto cycle, proceeding cyclically from $A \rightarrow B \rightarrow C \rightarrow D \dots$. The blue shaded area has units of energy and represents the net heat per cycle pumped away from the cold load at T_C . The low degeneracy subband state is designated with the line g_1 and the high degeneracy g_2 . The cycle is comprised of (A) Adiabatic expansion, (B) Isochoric heat withdrawn from the cold load, (C) Adiabatic compression, and (D) Isochoric heat ejected to the heat sink.

In the Otto cycle calculation below, we determine that MHz to GHz cycle frequencies can supply sufficient cooling power to compensate for parasitic heat loads, with excess cooling power to operate as a refrigerator. This refrigeration power can be used, for example, to overcome heat leaks from multiple electrical leads attached to a device targeted for refrigeration or from incident infrared radiation entering a detector window. For a given operating frequency f and heat sink temperature T_H , the cooling power can be calculated from the shaded region of the T - S diagram of Fig. 2,

$$P_c = f \int_{S_1}^{S_2} T_{g_2}(S) dS = f \frac{K}{2g_2} [(g_2 T_{e,C})^2 - (g_1 T_{e,H})^2]. \quad (2)$$

The primary source of electron heating in the device that will counteract this cooling power is direct electron-phonon coupling in the quantum well. It has been shown theoretically¹⁵ and experimentally¹⁶ that the local heat exchange from phonons at T_{ph} to electrons at T_e follows a power law,

$$\dot{Q}_{e-ph} = 3.3 \times 10^6 \frac{A_{QW}}{L\sqrt{n}} \int_0^L T_{ph}^5(x) - T_e^5 dx, \quad (3)$$

where n is the quantum well electron density. The position-dependent phonon temperature is $T_{ph}(x)$, where x measures the length from the hot side at $x = 0$ to the cold side at $x = L$ shown in gray at the bottom of Fig. 1a. On the other hand, the electrons are expected to have much faster thermal diffusion times than the phonons and are therefore modeled as having uniform temperature T_e across the width of the quantum well. The heat flow density through the lattice is $\dot{q}_{ph} = -\kappa_{ph}(x) \frac{dT_{ph}(x)}{dx}$

is approximated as being time independent under steady-state operation of the refrigerator. The thermal conductivity of the lattice follows a power law, $\kappa_{ph} \propto T_{ph}^3$. Integrating both sides of this steady-state heat flow expression across the length of the device from $x(T_C)$ to $x(T_H)$ results in the following expression for the phonon temperature as a function of position for a fixed T_H heat sink temperature,

$$T_{ph}(x, T_C) = \sqrt[4]{(T_C^4 - T_H^4) \frac{x}{L} + T_H^4}. \quad (4)$$

The local phonon temperature described in Eq. (4) will create a phonon backflow of heat from hot to cold reservoirs. The heat flow through the substrate phonons due to the temperature gradient is modeled as a one-dimensional heat flow described by the integral of the phonon thermal conductivity $\kappa_{ph} = \frac{1}{3} C_{ph} v_{ph} l_{ph}$ across the length of the sample, where v_{ph} and l_{ph} are the temperature-independent phonon sound velocity and mean free path, respectively, and $C_{ph}(x) = 2\pi^2 k_B^4 T^3 / (5\hbar^3 v_{ph}^3)$ is the phonon specific heat. For the total heat flow, this gives

$$\dot{Q}_S = \frac{Wt}{L_G + 2L_{hs}} \frac{\pi^2 k_B^4 l_{ph}}{30\hbar^3 v_{ph}^2} (T_H^4 - T_C^4), \quad (5)$$

where W , t , L_{hs} are the sample width, substrate thickness, and heat switch gate length, respectively. Calculations assume an experimentally reasonable 100 μm thinned substrate which can be achieved by mechanically or chemically thinning the sample, and even thinner micron-scale substrates can be achieved with remote epitaxial growth¹⁷, thereby reducing the cross-sectional area for the substrate phonon back-flow.

The only source of Joule heating comes from electrons depleting and repopulating the heat-switch gates, which can be reduced by including an oppositely biased reservoir gate immediately next to the heat-switch gate of equal dimensions whose accumulated charge can accommodate the depleted charge under the heat switch. With such a design, Joule heating J is given by

$$J = I^2 R = 2f^2 \frac{ne}{\mu} L_{hs}^3 W, \quad (6)$$

where L_{hs} , f , μ , n , and e are the length of the heat switch gates, operating frequency, the quantum well electron density, electron mobility, and electron charge, respectively.

The upper bound for the frequency of operation will be set by the time timescale associated with the diffusion of the electronic heat along the QW length L to achieve thermal equilibration of the central QW electrons with the cold load or the heat sink, respectively. This timescale is given by $\tau_q = L^2/\alpha$, implying a frequency-dependent thermal diffusion length:

$$L_q^2(f) = \frac{\alpha}{2f}. \quad (7)$$

with electron thermal diffusivity constant $\alpha = \frac{2}{3} \frac{\mu E_F}{e}$, whereby the thermal diffusion frequency is $f = 2/\tau_q$, since the thermal equilibration has to occur twice per cycle – once for cold-load equilibration, and once for heat-sink equilibration. The

diffusion length $L_q(f)$ represents an upper bound for a device operating with given frequency f , thus choosing $L = L_q(f)$ provides maximum cooling power. By adjusting the width W in order to hold the total device area A_{QW} of the central heat-pump region constant, we can simplify the geometry to $W(f) = A_{QW}/L(f)$, which gives the optimal geometry for a device operating at any given frequency.

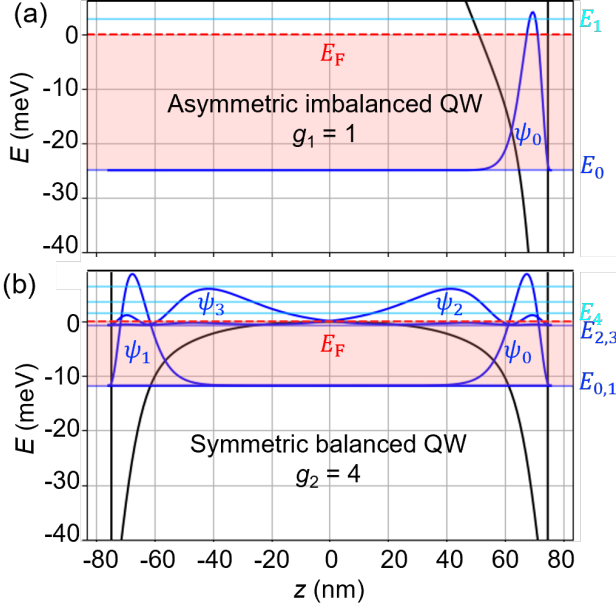


FIG. 3. Self-consistent Hartree calculations of (a) the asymmetric, imbalanced and (b) symmetric, balanced condition for a 150 nm-wide GaAs QW as controlled by front- and back-piston gates. For the imbalanced QW only the ground state wavefunction at energy E_0 is occupied, resulting in a subband degeneracy of $g_1 = 1$. The balanced QW, on the other hand, has both the ground state $E_{0,1}$ and first excited state $E_{2,3}$ degenerate subbands from opposite interfaces of the quantum well occupied, resulting in a fourfold subband degeneracy of $g_2 = 4$.

IV. MATERIAL AND DEVICE PARAMETERS

We calculate the viability of net cryogenic cooling power using a GaAs quantum well as an example. An ultra-wide quantum well-width $d_{QW} = 150$ nm is chosen to maximize the ratio of degeneracy factors g_1 and g_2 . Figure 3 shows a self-consistent Hartree calculation of quantum well subband energies¹⁸. When imbalanced with a large positive voltage on the front- and large negative voltage on the back-piston gates, a sharp triangular quantum well is formed at the front interface, shown in Fig. 3a. A density of $n = 10^{12}$ cm⁻² electrons in this GaAs quantum well with an effective mass of $m^* = 0.067m_0$ will populate only the lowest subband, with energy E_0 in the Hartree calculations of Fig. 3a. Note that the next nearest subband E_1 lies above the Fermi energy and is therefore unpopulated. When this same density is balanced by compensating front- and back-piston gate voltages to a square-well

configuration for the bare potential, the Coulomb repulsion of the electrons results in two symmetric triangular wells at the opposite corners of the well, Fig. 3b. These electrons together populate four subbands: the ground states E_0, E_1 and the first excited states E_2, E_3 in the right and left triangular wells, respectively. Thus, the same density of electrons in this wide quantum well can therefore be tuned from $g_1 = 1$ to $g_2 = 4$ subband degeneracy.

V. COOLING POWER

With the above model, the cooling power P_C of the Otto cycle refrigerator can be estimated, as well as the net cooling power P_{net} considering the heat loss terms defined earlier in the Letter,

$$P_{net} = P_C - J - \dot{Q}_{e-ph} - \dot{Q}_S. \quad (8)$$

For a range of heat sink temperatures $T_H = 3$ mK to 300 mK, Fig. 4 shows the calculated maximum net cooling power P_{max} at optimal device length $L(f)$ from Eq. (7) and frequency f at each T_C for a subband degeneracy refrigerator with $g_2:g_1 = 4:1$ and $L_{hs} = 1$ μ m heat switch gates. Simulations assume a quantum well with electron density $n = 1 \times 10^{12}$ cm⁻², electron mobility $\mu = 20 \times 10^6$ cm²/Vs¹⁹⁻²² known to be achievable below 1 K²³, and GaAs electron effective mass $m^* = 0.063m_0$. Substrate parameters are thickness $t = 100$ μ m, phonon velocity $v_{ph} = 4000$ m/s, and phonon mean-free path $l_{ph} = 1$ μ m²⁴. The calculations in Fig. 4a shows that this simple, single stage cooler can yield up to $P_{net} = 45$ μ W of net cooling power per $A_{QW} = 1$ cm² of device area at $T_H = T_C = 300$ mK and consistently supply several microwatts per cm² of cooling with $T_H \geq 100$ mK. In Fig. 4b, we see such a device can provide tens of nanowatts of cooling per cm² with T_H as low as 30 mK. Volumetric cooling could be realized by vertically stacking 100 devices, each of thickness $t = 100$ μ m thick, electrically connected in parallel, allowing one to consider a volumetric cooling power per unit device volume. Multiplying the P_{max} power per unit area in Fig. 4 by $1/t = 100$ /cm yields such a volumetric cooling power per unit volume. These calculations suggest we can achieve $P_{net} = 4.5$ mW/cm³ of volumetric cooling power density at hot side $T_H = 300$ mK.

VI. DISCUSSION

The solid-state refrigeration described here would initially serve to enhance cooling power near base temperature in tandem with a dilution refrigerator. To eventually compete with dilution refrigeration, cascaded multistage designs must be considered to allow for higher hot-side temperatures while achieving greater thermal differentials to colder base temperatures. The lateral design of the subband degeneracy refrigerator could be particularly well-suited for cascading, allowing for simple, monolithic, planar cascade designs where the heat sink of the former stage serves as the cold load of the latter stage.

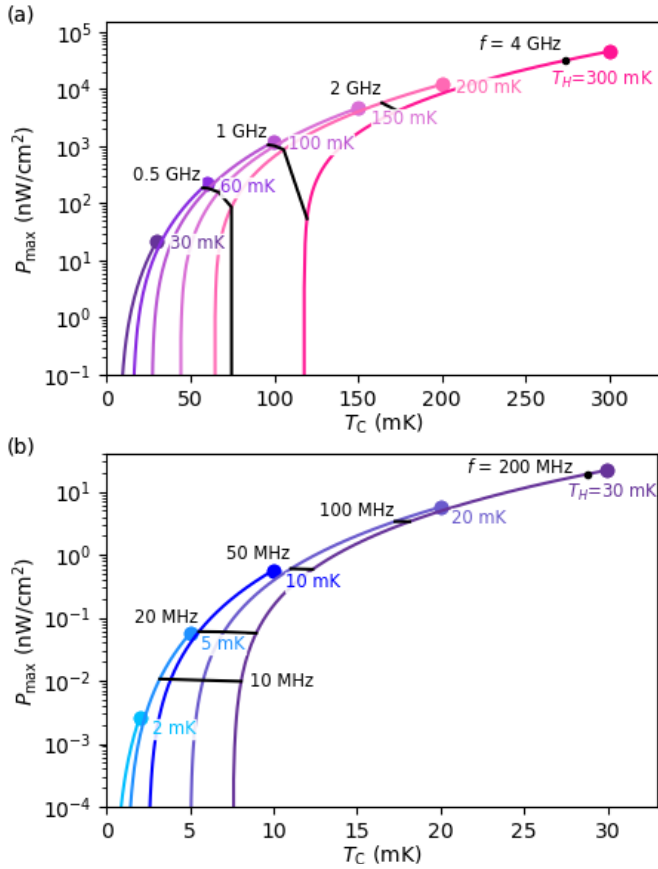


FIG. 4. Calculated maximum net cooling power P_{\max} as a function of the cold-side base temperature T_C for various heat sink temperatures T_H represented by colored curves between (a) 30 to 300 mK for the higher temperature range normally achievable in dilution refrigerators and (b) 2 to 30 mK for the lower temperature range, whose lowest temperatures typically require demagnetization refrigerators. Black curves indicate lines of constant cycling frequency f . Colored dots show maximum cooling power for the T_H curve of corresponding color.

Alternatively, the subband degeneracy refrigerator could be paired with other solid state cooling mechanisms such as superconducting-insulating-normal metal junction cooling to achieve a composite cascaded solid-state alternative to dilution refrigeration^{25,26}. Other thermodynamic heat pump cycles besides the Otto cycle may lead to improved cooling efficiency or increased cooling power at higher temperatures where electron-phonon coupling is enhanced. This proposed device therefore represents an initial candidate low-temperature stage for future exploration of solid-state refrigeration.

ACKNOWLEDGMENTS

This material is based upon work supported by the U.S. Department of Energy, Office of Science, National Quantum Information Science Research Centers, Superconducting Quantum Materials and Systems Center (SQMS) under the contract No. DE-AC02-07CH11359. T.D. thanks the support of URAP

funding from the Office of Undergraduate Research, Northwestern University. The authors also thank Lucia Steinke (U. Florida) for insightful conversations.

- ¹J. P. Gardner, J. C. Mather, M. Clampin, R. Doyon, M. A. Greenhouse, H. B. Hammel, J. B. Hutchings, P. Jakobsen, S. J. Lilly, K. S. Long, *et al.*, “The james webb space telescope,” *Space Science Reviews* **123**, 485–606 (2006).
- ²R. Agnese, A. J. Anderson, M. Asai, D. Balakishiyeva, R. B. Thakur, D. Bauer, J. Beaty, J. Billard, A. Borgland, M. Bowles, *et al.*, “Search for low-mass weakly interacting massive particles with supercdms,” *Physical review letters* **112**, 241302 (2014).
- ³L. V. Levitin, H. van der Vliet, T. Theisen, S. Dimitriadis, M. Lucas, A. D. Corcoles, J. Nyéki, A. J. Casey, G. Creeth, I. Farrer, *et al.*, “Cooling low-dimensional electron systems into the microkelvin regime,” *Nature communications* **13**, 1–8 (2022).
- ⁴P. Das, R. Ouboter, and K. Taconis, “A realization of a london-clarkemendoza type refrigerator,” in *Low Temperature Physics LT9* (Springer, 1965) pp. 1253–1255.
- ⁵E. Figueroa-Feliciano, A. J. Anderson, D. Castro, D. C. Goldfinger, J. Rutherford, M. E. Eckart, R. L. Kelley, C. A. Kilbourne, D. McCammon, K. Morgan, *et al.*, “Searching for keV sterile neutrino dark matter with x-ray microcalorimeter sounding rockets,” *The Astrophysical Journal* **814**, 82 (2015).
- ⁶J. Adams, R. Baker, S. Bandler, N. Bastidon, M. Danowski, W. Doriese, M. Eckart, E. Figueroa-Feliciano, D. Goldfinger, S. Heine, *et al.*, “First operation of tes microcalorimeters in space with the micro-x sounding rocket,” *Journal of Low Temperature Physics* **199**, 1062–1071 (2020).
- ⁷G. L. Pollack, “Kapitza resistance,” *Reviews of modern physics* **41**, 48 (1969).
- ⁸M. Grayson, “Cryogenic solid state heat pump,” *International Patent PCT/US2020/03 1082* (2022).
- ⁹L.-M. Duan and G.-C. Guo, “Reducing decoherence in quantum-computer memory with all quantum bits coupling to the same environment,” *Physical Review A* **57**, 737 (1998).
- ¹⁰L. G. Rego and G. Kirczenow, “Electrostatic mechanism for cooling semiconductor heterostructures,” *Applied physics letters* **75**, 2262–2264 (1999).
- ¹¹J. Bardeen, G. Rickayzen, and L. Tewordt, “Theory of the thermal conductivity of superconductors,” *Physical Review* **113**, 982 (1959).
- ¹²C. Satterthwaite, “Thermal conductivity of normal and superconducting aluminum,” *Physical Review* **125**, 873 (1962).
- ¹³C. Wu, *Thermodynamic cycles: computer-aided design and optimization* (CRC Press, 2003).
- ¹⁴N. Ashcroft and N. Mermin, *Solid State Physics* (Saunders College, Philadelphia, 1976).
- ¹⁵P. J. Price, “Hot electrons in a gaas heterolayer at low temperature,” *Journal of Applied Physics* **53**, 6863–6866 (1982).
- ¹⁶A. Mittal, R. Wheeler, M. Keller, D. Prober, and R. Sacks, “Electron-phonon scattering rates in gaas/algaas 2deg samples below 0.5 k,” *Surface Science* **361-362**, 537–541 (1996).
- ¹⁷Y. Kim, S. S. Cruz, K. Lee, B. O. Alawode, C. Choi, Y. Song, J. M. Johnson, C. Heidelberg, W. Kong, S. Choi, *et al.*, “Remote epitaxy through graphene enables two-dimensional material-based layer transfer,” *Nature* **544**, 340–343 (2017).
- ¹⁸H. Hebal, Z. Koziol, S. Lisesivdin, and R. Steed, “General-purpose open-source 1d self-consistent schrödinger-poisson solver: Aestimo 1d,” *Computational Materials Science* **186**, 110015 (2021).
- ¹⁹C. Reichl, J. Chen, S. Baer, C. Rössler, T. Ihn, K. Ensslin, W. Dietsche, and W. Wegscheider, “Increasing the $\nu=5/2$ gap energy: an analysis of mbe growth parameters,” *New Journal of Physics* **16**, 023014 (2014).
- ²⁰M. Banerjee, M. Heiblum, V. Umansky, D. E. Feldman, Y. Oreg, and A. Stern, “Observation of half-integer thermal hall conductance,” *Nature* **559**, 205–210 (2018).
- ²¹E. Hwang and S. D. Sarma, “Limit to two-dimensional mobility in modulation-doped gaas quantum structures: How to achieve a mobility of 100 million,” *Physical Review B* **77**, 235437 (2008).
- ²²M. J. Manfra, “Molecular beam epitaxy of ultra-high-quality algaas/gaas heterostructures: enabling physics in low-dimensional electronic systems,” *Annu. Rev. Condens. Matter Phys.* **5**, 347–373 (2014).
- ²³D. G. Schlom and L. N. Pfeiffer, “Upward mobility rocks!” *Nature materials* **9**, 881–883 (2010).

- ²⁴W. Fon, K. Schwab, J. Worlock, and M. Roukes, "Phonon scattering mechanisms in suspended nanostructures from 4 to 40 k," *Physical review B* **66**, 045302 (2002).
- ²⁵M. Leivo, J. Pekola, and D. Averin, "Efficient peltier refrigeration by a pair of normal metal/insulator/superconductor junctions," *Applied physics letters* **68**, 1996–1998 (1996).
- ²⁶G. C. O'Neil, P. J. Lowell, J. M. Underwood, and J. N. Ullom, "Measurement and modeling of a large-area normal-metal/insulator/superconductor refrigerator with improved cooling," *Physical Review B* **85**, 134504 (2012).